


## Article

# Artificial Neural Networks for the Prediction of the Reference Evapotranspiration of the Peloponnese Peninsula, Greece

Stavroula Dimitriadou and Konstantinos G. Nikolakopoulos \* 

Department of Geology, University of Patras, 26504 Patras, Greece; sdhm@upatras.gr

\* Correspondence: knikolakop@upatras.gr; Tel.: +30-261-099-7592

**Abstract:** The aim of the study was to investigate the utility of artificial neural networks (ANNs) for the estimation of reference evapotranspiration (ET<sub>o</sub>) on the Peloponnese Peninsula in Greece for two representative months of wintertime and summertime during 2016–2019 and to test if using fewer inputs could lead to satisfactory predictions. Datasets from sixty-two meteorological stations were employed. The available inputs were mean temperature (T<sub>mean</sub>), sunshine (N), solar radiation (R<sub>s</sub>), net radiation (R<sub>n</sub>), vapour pressure deficit (es-ea), wind speed (u<sub>2</sub>) and altitude (Z). Nineteen Multi-layer Perceptron (MLP) and Radial Basis Function (RBF) models were tested and compared against the corresponding FAO-56 Penman Monteith (FAO PM) estimates of a previous study, via statistical indices. The MLP1 7-2 model with all the variables as inputs outperformed the rest of the models (RMSE = 0.290 mm d<sup>-1</sup>, R<sup>2</sup> = 98%). The results indicate that even ANNs with simple architecture can be very good predictive models of ET<sub>o</sub> for the Peloponnese, based on the literature standards. The MLP1 model determined T<sub>mean</sub>, followed by u<sub>2</sub>, as the two most influential factors for ET<sub>o</sub>. Moreover, when one input was used (T<sub>mean</sub>, R<sub>n</sub>), RBFs slightly outperformed MLPs (RMSE < 0.385 mm d<sup>-1</sup>, R<sup>2</sup> ≥ 96%), which means that even a sole-input ANN resulted in satisfactory predictions of ET<sub>o</sub>.

**Keywords:** multilayer perceptron; MLP; radial basis function; RBF; ANN; neural networks; reference evapotranspiration; Peloponnese; Greece



**Citation:** Dimitriadou, S.; Nikolakopoulos, K.G. Artificial Neural Networks for the Prediction of the Reference Evapotranspiration of the Peloponnese Peninsula, Greece. *Water* **2022**, *14*, 2027. <https://doi.org/10.3390/w14132027>

Academic Editor: Guido D'Urso

Received: 25 May 2022

Accepted: 21 June 2022

Published: 24 June 2022

**Publisher's Note:** MDPI stays neutral with regard to jurisdictional claims in published maps and institutional affiliations.



**Copyright:** © 2022 by the authors. Licensee MDPI, Basel, Switzerland. This article is an open access article distributed under the terms and conditions of the Creative Commons Attribution (CC BY) license (<https://creativecommons.org/licenses/by/4.0/>).

## 1. Introduction

Reference Evapotranspiration (ET<sub>o</sub>) is a key climate parameter investigated in the frame of climate crisis and water resources management [1–4]. Moreover, ET<sub>o</sub> has an effect on the productive sector of agriculture [5]. In particular, the precision irrigation techniques and the decision-making irrigation systems demand accurate ET<sub>o</sub> values [6]. Therefore, the importance of effective estimation and prediction methods of ET<sub>o</sub> is crucial [7,8].

The necessity of acquiring ET<sub>o</sub> values led to the development of several methods of estimation, ranging from simple empirical or physically based models [9,10] to complex neuro-fuzzy and machine learning algorithms [11–47]. The methods incorporate data from meteorological stations or, due to the scarcity of the former, remotely sensed data [48–58]. The FAO-56 Penman Monteith (FAO PM) equation requires numerous meteorological variables for effective application [59,60]. Even the more refined empirical methods of ET<sub>o</sub>, such as Valiantzas' equations [61], share a common denominator; the more meteorological inputs, the higher the accuracy of ET<sub>o</sub> [62]. On the other hand, there are empirical methods requiring limited climatic variables (e.g., the Hargreaves'-Samani equation). However, the accuracy of these methods, compared to FAO PM, is limited and performance in some cases has been reported to be season-dependent [63]. The unavailability of input data is a global issue, due to the high cost of equipping and running meteorological stations, especially for developing countries. Thus, reducing the number of inputs for the predicting models to only trivial parameters is highly recommended [64]. Those parameters can be air temperature (minimum, maximum and mean values) plus parameters that can

be either measured or easily computed based on latitude and Julian day (e.g., sunshine, solar radiation, net radiation, vapor pressure deficit and wind speed) [59]. Computing the missing parameters is a commonly used practice in ETo research [61,65]. However, even if input parameters are trivial, their inner relationships are non-linear and complex. Among different methods, Artificial Neural Networks (ANNs) stand out for their capability to model complex non-linear relationships. ANNs demand short real-time control and computational effort [66]. Hence, they are considered as a suitable approach to model ETo.

Artificial neural networks are utilized in a broad spectrum of applications. ANN architectures consist of one input layer (including several input variables), multiple hidden layers and one output layer. The hidden layers consist of several neurons (or nodes) and each neuron can have multiple inputs and one output. The output of each neuron is connected to a neuron of the successive layer via a synapse. Each synapse is a link which has a particular weight to represent the strength of the connection between two successive neurons. After computing the sum of all weighted inputs, neurons transfer this sum into an output via an activation function. This output is fed to the next layer. The output of the network is computed by the last neuron of the network [67]. Multi-layer Perceptron (MLP) and Radial Basis Function (RBF) are common ANNs with capabilities in ETo forecasting [68–72].

Trajkovic (2009) [68], based on Trajkovic et al. (2003) [69], demonstrated that an RBF model with only two input variables is able to predict ETo with greater accuracy than FAO PM, amongst other equations. Kumar et al. (2020) [70] tested two models with five and two input variables, respectively, for the Himalayan region, employing ground-based data from forty-seven stations. They found that MLP could satisfactorily predict ETo even with limited inputs. Tabari et al. (2012) [71] investigated four MLP models with four, three and two input variables, for a semi-arid region in Iran. They concluded that the model with the most inputs resulted in the most accurate predictions of ETo and that tanh was the best activation function in all cases. Sattari et al. (2021) tried ten combinations of input variables (from eight to one inputs) [72]. The best performance yielded an  $R^2 = 0.978$ . Shamshirband et al. (2016) [73] used data from twelve meteorological stations in Serbia for optimizing an ANN with very low error levels, but an  $R^2$  below 0.97. Gavili et al. (2017) [74] tested soft computing methods versus empirical ones and deduced that the former exhibited better performance in modeling ETo. Amongst these methods, the ANN had the best performance. As far as Greece is concerned, Diamantopoulou et al. (2011) [75] tested two ANNs to estimate daily ETo with limited meteorological data, separately for four meteorological stations in the Northern Greece. The best results obtained an  $RMSE = 0.545 \text{ mm d}^{-1}$  and an  $R^2 = 95.7\%$ . Antonopoulos et al. (2016) [76] applied ANNs also in the Northern Greece (Lake Vegoritis) to predict ETo. For years 2003 and 2004, they obtained:  $RMSE = 0.69 \text{ mm d}^{-1}$ ,  $R^2 = 79.2\%$  and  $RMSE = 1.09 \text{ mm d}^{-1}$ ,  $R^2 = 82.8\%$ , respectively. Antonopoulos and Antonopoulos (2017) [77], in consecutive research in the same study area, trained ANNs with datasets from one meteorological station (Amyntaio) over the period 2009–2013 to estimate ETo. Their best results yielded an  $RMSE = 0.574 \text{ mm d}^{-1}$  and an  $R^2$  around 97.2%, while the indices' values were slightly deteriorated for lesser (i.e., three and two) inputs.

Although ANN is considered a suitable method to model ETo, the literature lacks in studies of areas with interchangeable land use/land cover (LU/LC) and relief characteristics over short distances. In those areas the performance of a model predicting ETo would be challenging in terms of accuracy and seasonal consistency. Moreover, the number of meteorological stations employed in the literature is usually low compared to the corresponding study area, which leads to a coarser spatial representation of the climate variables. Lastly, as shown above, there are only a few applications of ANNs for ETo prediction in Greece in the literature.

The aim of the study was to investigate whether ANNs could predict ETo satisfactorily close to the reference method (FAO PM) in the Peloponnese, Greece, for the selected period. The study also aimed to determine the model that best fits the data, based on the

literature standards, and to indicate the most influential factors on ETo. This study examines nineteen MLP and RGB (ANN) models utilizing sixty-two meteorological stations in the Peloponnese peninsula in Southwestern Greece (Table A1). The Peloponnese peninsula is a study area with distinguished differences over short distances. Empirical methods applied across the area in a previous study [63] showed inferior performance in terms of accuracy, especially for August (summertime). A further objective was to examine whether fewer input variables would produce satisfactory predictions of ETo in terms of accuracy. Therefore, the number of inputs of the models were consecutively reduced to examine whether fewer than the seven available inputs, or even a sole input, could predict ETo acceptably. The novelty of the study is twofold: it is the first time that ANNs are used to predict the ETo across a large area of Southern Greece, which includes elevation, relief and LU/LC interchanges that are challenging in terms of the consistency of model performance. Even more challenging is the usage of continuous climate datasets over a recent four-year period, instead of datasets for individual days or short intervals. In addition, the exploitation of a dense meteorological station network, instead of a couple of stations, enhances the significance of the results. A good performance from ANNs, despite the aforementioned difficulties, would prove the flexibility and the potential of ANNs in ETo modeling. The latter would be useful in cases where there is a shortage of climate data. Moreover, it could save time and decrease computational load for interdisciplinary research purposes.

## 2. Materials and Methods

### 2.1. The Study Area

The Peloponnese is a peninsula in Southwestern Greece that occupies about 1/6th of the Greek territory (21,439 km<sup>2</sup>), with a population of 1086.935 (census 2011; <https://www.statistics.gr/el/statistics/-/publication/SAM03/2011> (accessed on 10 March 2022)). A large part is covered by high hills and mountains, running NW to SE, with an elevation up to 2407 m. Lithology, tectonic activity and climate conditions have resulted in the relief formation of the study area. A well-developed hydrographic network, though with few large rivers, has formed [78]. Based on the latest Copernicus LU/LC classification, the widest urban area is located at the northmost edge [79]. In addition to urban areas, the main LU/LC types are forest and transitional vegetation, as well as crop plots covering the plains (Figure 1). The broadest plain lies over the western coastal part. According to Köppen-Geiger's classification, the climate of the Peloponnese is Mediterranean warm temperate with dry summers and mild winters (Csa) [80]. The annual normal measurements (1971–2000) of air temperature, precipitation and sunshine range between 8–20 °C, 400 to over 2000 mm and 1900–3100 h, respectively (<http://climatlas.hnms.gr/sdi/?lang=EN> (accessed on 27 April 2022)).

### 2.2. Methods

Meteorological datasets of daily measurements from sixty-two stations under the National Observatory of Athens, for the months August and December of 2016–2019, were utilized (Table A1). These months and years were selected for the application of ANNs in methodological consistency with our previous study [63], where ETo was computed for the Peloponnese by FAO PM, our reference method. In that study, August and December had been selected as typical months of summer and winter, respectively. FAO PM has been widely used as a reference method to estimate ETo in studies investigating ANNs, either as the only reference method [10,70,81] or combined with direct methods [82]. Multi-Layer Perceptron (MLP) and Radial Basis Function (RBF) ANN models were examined in this study. Nineteen combinations of input variables were tested (from seven inputs to one input) with both MLP and RBF models. The inputs included climate and non-climate (such as altitude) variables that affect ETo [83], namely, solar radiation (Rs), net radiation (Rn), sunshine hours (N), mean air temperature (Tmean), vapour pressure deficit (es-ea), wind speed at 2 m from the surface (u<sub>2</sub>) and altitude (Z). The first three were previously calculated

as functions of the station latitude and the Julian day, as in Zanetti et al. (2008) [36]. Based on Rahimikhoob (2020) [84], the input combinations were subsequently limited, aiming to explore the possibility of producing acceptably accurate predictions of ETo with fewer variables than the available seven or even with a sole input variable (such as Tmean or Rn). About three fifths of the sample data were used for training and the other two fifths were used for testing and validation (about one fifth each) [40]. The tested architecture was based on the trial-and-error method and the ANNs were trained using the Levenberg-Marquardt algorithm [40,41]. Hyperbolic tangent (Equation (1); [85]) was the utilized activation function, based on the literature [71,86]. The hyperbolic tangent, along with the sigmoid function, is a non-linear function widely used as an activation function in ANNs [85]. The hyperbolic tangent exhibits the advantage of giving higher enhancement to the negative values. The output of the former spans in  $[-1, 1]$  while the sigmoid outputs are only half of the previous ( $[0, 1]$ ) [87].

$$\text{Tanh}(x) = \frac{e^x - e^{-x}}{e^x + e^{-x}} \tag{1}$$

The values predicted by the ANN models were then compared against the values by FAO PM via statistical indices that were computed during the training, testing and validation phases (SSE, RE) (Table 1). Furthermore, the error levels between predicted and reference values have been computed via measures such as Root Mean Square Error (RMSE,  $\text{mm d}^{-1}$ ), Normalized Root Mean Square Error (NRMSE, %), Mean Absolute Error (MAE,  $\text{mm d}^{-1}$ ), Mean Bias (MB,  $\text{mm d}^{-1}$ ) and Sum of Squares Error (SSE,  $\text{mm}^2 \text{d}^{-1}$ ) (Table 1). The error values depict the magnitude of the computed ETo values, except from NRMSE, which is expressed in \*100%. Mean Bias is a signed measure so that, in addition to producing the Mean Bias Error (MBE = |MB|), it provides some extra information; the minus sign depicts that the reference ETo value (by FAO PM) is greater than the model predicted value and vice versa. Moreover, three measures that express correlation, strength of fit or agreement were used, namely, Pearson correlation coefficient (Pearson’s r), coefficient of determination ( $R^2$ ) and Index of Agreement (IoA) (Table 1).

**Table 1.** Formulae of the indices utilized to evaluate the performance of the examined ANN models.

Performance Evaluating Indices		
$\text{RMSE} = \sqrt{\frac{\sum_{i=1}^n (p_i - o_i)^2}{n}}$	$\text{NRMSE} = \frac{\sqrt{\frac{\sum_{i=1}^n (p_i - o_i)^2}{n}}}{\bar{o}}$	$\text{IoA} = 1 - \frac{\sum_{i=1}^n (p_i - o_i)^2}{\sum_{i=1}^n ( p_i - \bar{o}  +  o_i - \bar{o} )^2}$
$\text{MAE} = \frac{\sum_{i=1}^n  p_i - o_i }{n}$	$\text{MB} = \frac{\sum_{i=1}^n (p_i - o_i)}{n}$	$r = \frac{\sum_{i=1}^n (p_i - \bar{p})(o_i - \bar{o})}{\sqrt{\sum_{i=1}^n (p_i - \bar{p})^2 \sum_{i=1}^n (o_i - \bar{o})^2}}$
$\text{SSE} = \sum_{i=1}^n (p_i - o_i)^2$	$\text{RE} = \left  \frac{p_i - o_i}{o_i} \right $	$R^2 = \left( \frac{n \sum_{i=1}^n p_i o_i - \sum_{i=1}^n p_i \sum_{i=1}^n o_i}{\sqrt{n \sum_{i=1}^n p_i^2 - (\sum_{i=1}^n p_i)^2} * \sqrt{n \sum_{i=1}^n o_i^2 - (\sum_{i=1}^n p_i)^2}} \right)^2$

In Table 1,  $p_i$  stands for the  $i$ th predicted value by an ANN,  $o_i$  stands for the  $i$ th observed value, which in this study is the  $i$ th reference value estimated by FAO PM,  $\bar{o}$  is the mean of the observed (reference) values and  $n = 290$  is the sample size.

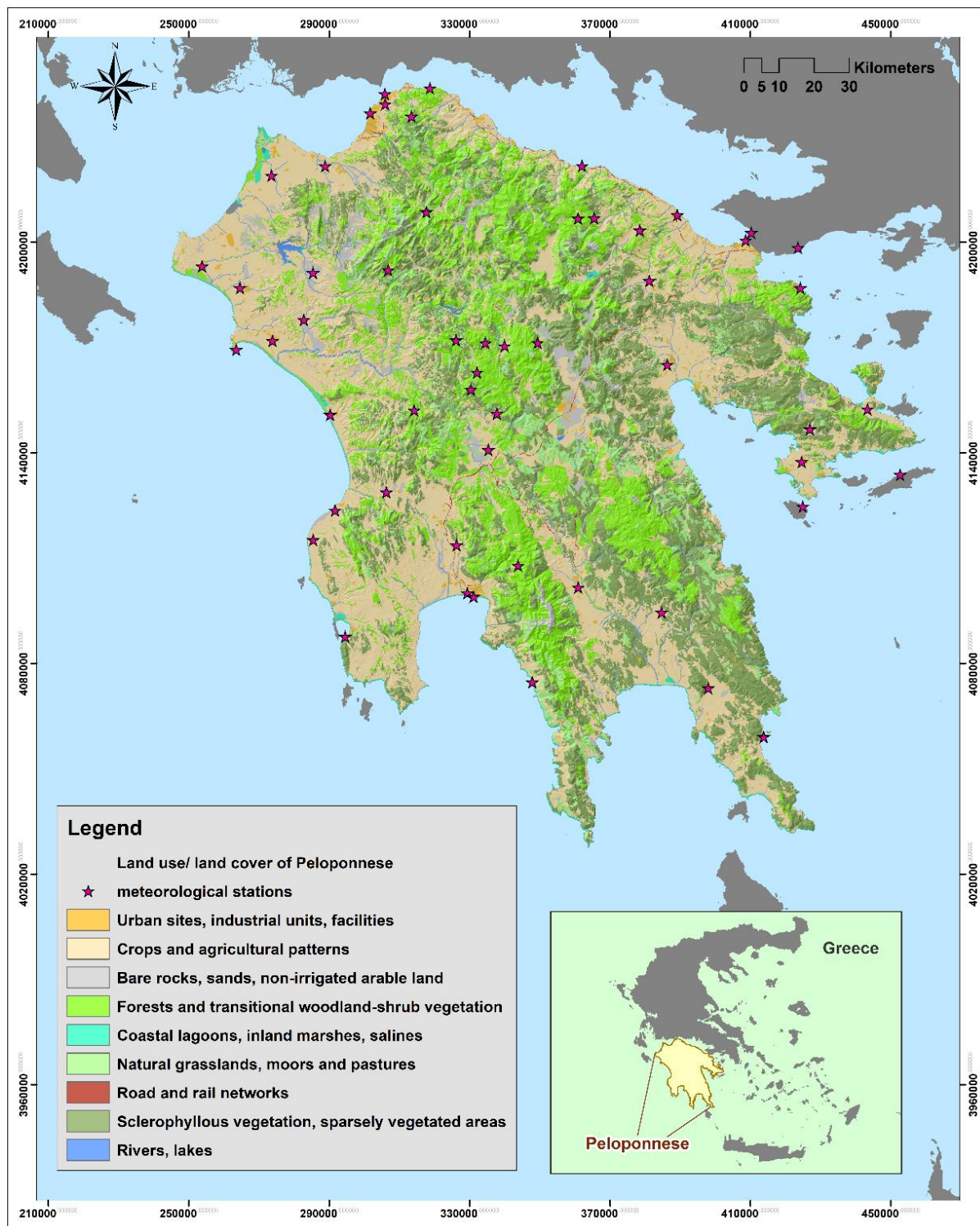


**Figure 1.** Land use/land cover map of the Peloponnese (Adapted with permission from Ref. [79] 2018, © European Union).

### 3. Results

In total, nineteen models with different input combinations were tested. The results are presented in Table 2.

**Table 2.** The examined ANN models (19) and the corresponding indices of performance.

ANN	Architecture	RMSE	NRMSE	MAE	MBE	R <sup>2</sup>	Pearson's r	IoA	SSE Testing	RE Testing	RE Hold-out
7 inputs: N, Rs, Rn, u <sub>2</sub> , es-ea, Tmean, Z											
<b>MLP1</b>	<b>7-2</b>	<b>0.290</b>	<b>0.086</b>	<b>0.217</b>	<b>0.017</b>	<b>0.980</b>	<b>0.990</b>	<b>0.995</b>	<b>0.695</b>	<b>0.027</b>	<b>0.022</b>
MLP2	7-4-3	0.305	0.090	0.230	0.024	0.978	0.989	0.994	0.573	0.021	<i>0.029</i>
RBF1	7-5	0.423	0.125	0.267	0.004	0.957	0.978	0.989	0.948	0.027	<i>0.100</i>
RBF2	7-9	0.333	0.098	0.246	−0.032	0.974	0.987	0.993	1.547	0.045	0.028
6 inputs: Rs, Rn, u <sub>2</sub> , es-ea, Tmean, Z											
MLP8	6-4	0.311	0.092	0.240	0.005	0.977	0.988	0.994	0.827	0.024	<i>0.025</i>
<b>MLP9</b>	<b>6-4-3</b>	<b>0.296</b>	<b>0.088</b>	<b>0.218</b>	<b>−0.008</b>	<b>0.979</b>	<b>0.989</b>	<b>0.995</b>	<b>1.188</b>	<b>0.035</b>	<b>0.024</b>
RBF3	6-9	0.318	0.094	0.232	0.016	0.976	0.988	0.994	0.623	0.026	0.022
4 inputs: Rs, u <sub>2</sub> , es-ea, Tmean and 4' inputs: Rn, u <sub>2</sub> , es-ea, Tmean											
MLP7	4-3	0.309	0.091	0.233	−0.002	0.977	0.989	0.994	0.543	0.020	<i>0.027</i>
MLP10	4-3-2	0.300	0.089	0.221	0.001	0.978	0.989	0.995	0.541	0.020	<i>0.028</i>
RBF4	4-10	0.406	0.120	0.263	−0.042	0.961	0.980	0.990	1.044	0.031	<i>0.092</i>
MLP3	4'-1	0.319	0.094	0.245	−0.025	0.976	0.988	0.994	0.459	0.160	<i>0.300</i>
3 inputs: Rn, u <sub>2</sub> , Tmean											
MLP5	3-1	0.314	0.093	0.244	−0.019	0.976	0.988	0.994	1.101	0.032	0.030
2 inputs: Rn, Tmean; 2' inputs: Rn, u <sub>2</sub> ; 2'' inputs: u <sub>2</sub> , Tmean											
MLP4	2-1	0.377	0.111	0.268	−0.023	0.966	0.983	0.991	1.443	0.042	0.034
MLP6	2'-1	0.343	0.101	0.268	0.026	0.972	0.986	0.093	0.961	0.037	0.028
<b>MLP13</b>	<b>2''-1</b>	<b>0.352</b>	<b>0.104</b>	<b>0.267</b>	<b>−0.008</b>	<b>0.970</b>	<b>0.985</b>	<b>0.992</b>	<b>0.819</b>	<b>0.029</b>	<b>0.029</b>
1 input: Tmean; 1' input: Rn											
MLP14	1-1	0.360	0.106	0.258	0.014	0.969	0.984	0.992	0.747	0.027	<i>0.041</i>
MLP16	1'-1	0.404	0.119	0.313	−0.014	0.961	0.980	0.990	0.594	0.030	<i>0.042</i>
RBF6	1-1	0.363	0.107	0.259	0.006	0.968	0.984	0.992	0.710	0.028	<i>0.033</i>
<b>RBF9</b>	<b>1'-1</b>	<b>0.383</b>	<b>0.113</b>	<b>0.298</b>	<b>−0.005</b>	<b>0.965</b>	<b>0.982</b>	<b>0.991</b>	<b>1.109</b>	<b>0.036</b>	<b>0.033</b>

Note: The values in italics (RE holdout column) indicate overtraining of the corresponding model. The models in bold exhibit performance that is discussed in detail. RMSE, MAE, MB are in mm d<sup>−1</sup> and SSE in mm<sup>2</sup> d<sup>−1</sup>.

As presented in Table 2, MLP1 7-2, with all the available parameters as inputs, appears to provide the best performance, expressed via the minimum error values in the testing and validation data and the maximum correlation and agreement indices (R<sup>2</sup>, Pearson's r and IoA) between prediction and reference values. The architecture is simple, consisting of one hidden layer with two neurons (Figure 2).

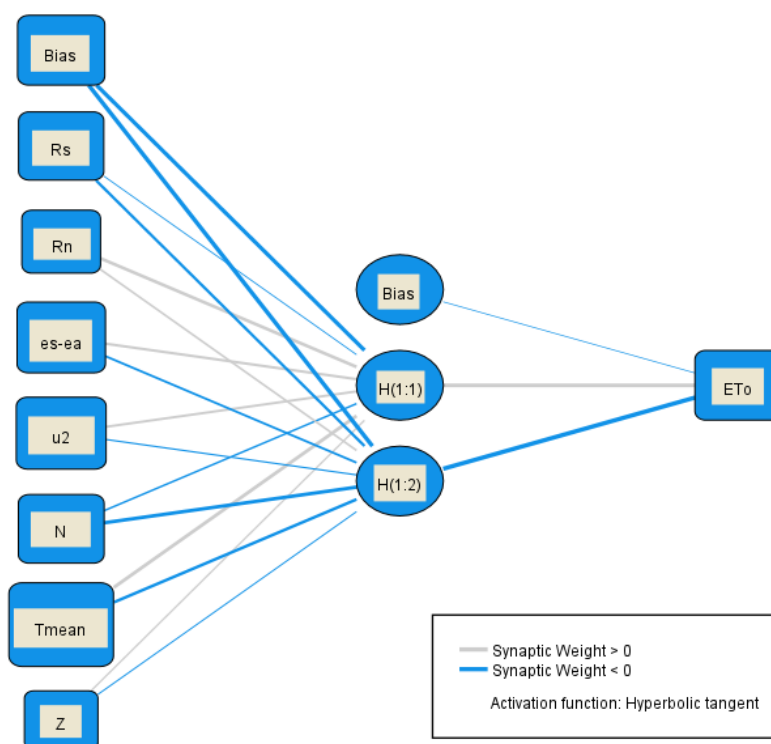


**Figure 2.** MLP1 model with the best performance on ETo predictions for the Peloponnese (August and December of 2016–2020).

The parameter-estimates of the MLP1 model are displayed in Table 3. As presented, the values of both the nodes and the hidden layers are not negligible values, a fact that constitutes one of the desirable characteristics of an ANN model.

**Table 3.** Parameter estimates of the model with the best performance (MLP1).

Predictor	Predicted		
	Hidden Layer 1		Output Layer
	H (1:1)	H (1:2)	ETo
(Bias)	−0.616	−0.638	
Rs	−0.010	−0.355	
Rn	0.397	0.173	
es-ea	0.224	−0.181	
u <sub>2</sub>	0.214	−0.049	
N	−0.100	−0.520	
Tmean	0.461	−0.394	
Z	0.059	−0.040	
Hidden Layer 1	(Bias)		−0.009
	H (1:1)		0.578
	H (1:2)		−0.867

As presented in Table 2, MLP9 6-4-3 follows closely the model with the superior performance (MLP1), except for the testing SSE value, which is almost double the corresponding MLP1 value. It is interesting that the MLP10 4-3-2 model, with only four inputs and two hidden layers, exhibits a performance very close to that of MLP1, with a couple of values (MBE and SSE) even better than those of MLP1. The added value is that it produces

almost the same values with only four basic parameters as inputs, specifically,  $R_s$ ,  $es-ea$ ,  $u_2$  and  $T_{mean}$ . The data of the aforementioned parameters are usually available either from meteorological stations or via remote sensing. Moreover, in the event of any missing data, the parameters can be easily computed [59]. It is obvious that the RBF network displays inferior performance to MLP for our data. RBF3 6-9 is the best among the RBF networks and fourth in the total rank of model performance. The relative errors of MLPs in the validation phase were between 2.2–4.2% for all trials, whereas for RBFs the relative errors lay between 2.8–10%. For the majority of the models, the holdout RE values were greater than the testing RE values, despite the satisfactory error levels (2.8–4.5%). This indicates that those models were overtrained towards the testing data.

The cases where only a sole basic parameter ( $T_{mean}$  or  $R_n$ ) was set as input seem noteworthy. In those cases, the RBF models exhibited better performance than the MLP ones. RBF9 ( $R_n$  as input) obtained  $RMSE = 0.383 \text{ mm d}^{-1}$  and  $R^2 = 96.5\%$  with  $RE = 3.3\%$ . In the case of  $T_{mean}$  as the sole input, the  $RMSE$  was around  $0.360 \text{ mm d}^{-1}$  and the  $R^2$  was above 96.7%. However, as previously commented, there was evidence of overtraining of some models (Table 2). Therefore, those models are not recommended. The influence of each climatic variable on  $ETo$  presented is considered important in respect of the ANN that best fits the data and bears interesting determination [14]. As shown in Figure 3, the most influential factor is  $T_{mean}$  followed by  $u_2$ . The third factor in the rank is vapour pressure deficit ( $es-ea$ ). Those results are aligned with the  $ETo$  estimates by FAO PM of the same period for the Peloponnese [63].

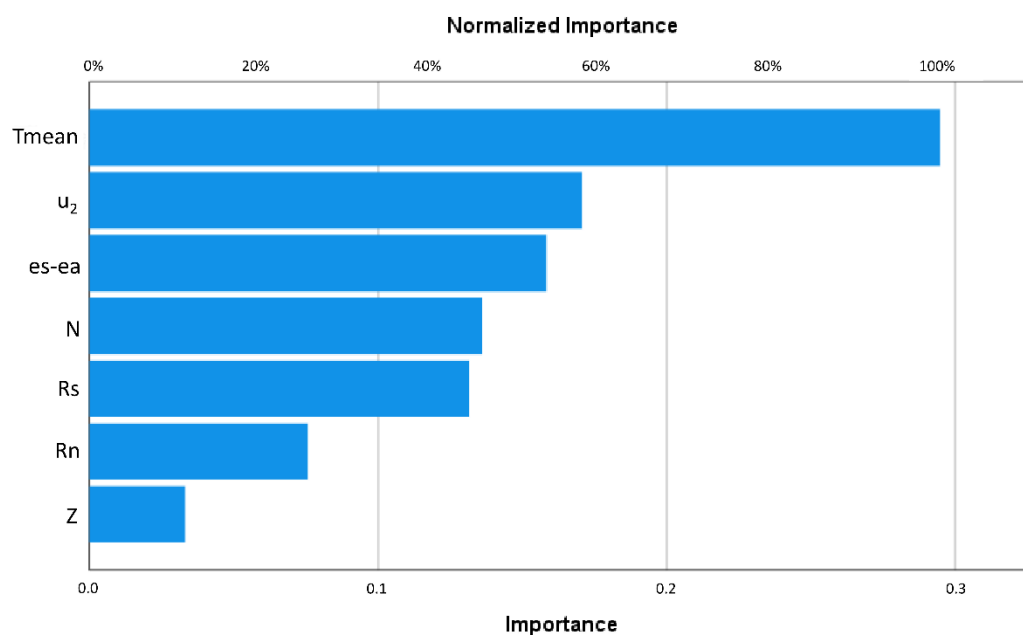


**Figure 3.** Normalized importance of the input variables of the model with the best performance (MLP1) in  $ETo$  prediction of the Peloponnese.

#### 4. Discussion

The determination of  $ETo$  is crucial for climate crisis research, hydrological cycle, water resources management and irrigation precision techniques. The available methods of estimation require the knowledge of numerous climate parameters, which means an increased cost. Since  $ETo$  includes complex and nonlinear relationships, ANNs have been proven to be a suitable modeling choice. In this study,  $ETo$  has been estimated via nineteen MLP and RBF ANN architectures, with different combination and number of inputs (from seven to one).

This period is interesting in the frame of the climate crisis, since it is recent and includes the first (2016) and second (2019) warmest years since the preindustrial era, which challenges the performance of ANNs.



For the majority of the trials, the RMSE was below  $0.4 \text{ mm d}^{-1}$  and the relative error of the testing phase was below 4%. MLPs performed generally better than RBFs for multiple inputs, whereas RBFs performed slightly better when only one input ( $R_n$  or  $T_{\text{mean}}$ ) was set. The model that best fits the reference values was that with the most input parameters and only one hidden layer (MLP1 7-2), bearing  $\text{RMSE} = 0.290 \text{ mm d}^{-1}$ ,  $R^2 = 98\%$  and RE of testing and validation phases equal to 2.7% and 2.2%, respectively. The different runs with the same input combination, but different model architecture, showed that any increase in the number of hidden layers and the number of neurons in the hidden layer exhibited negligible improvement in prediction accuracy. Those conclusions are in line with the findings by Tabari et al. (2012) [71]. The data of the seven used inputs can be easily derived, either by meteorological stations or via remote sensing, or can be easily computed as missing data by FAO guidelines [59]. However, during the trials, the number of the inputs was gradually limited in order to examine whether ANNs can provide satisfactory estimates of  $E_{\text{To}}$ , when incorporating only the most commonly available climate data. It is interesting that the MLP10 with four climate parameters as inputs exhibited results very close to the best model (MLP1). Moreover, models with two basic parameters as inputs, exhibited RMSE up to  $0.352 \text{ mm d}^{-1}$ , testing RE below 3% and  $R^2$  at least equal to 97% (MLP6, MLP13). When only one input was used (i.e.,  $T_{\text{mean}}$  or  $R_n$ ) in RBF models, the RMSE was below  $0.385 \text{ mm d}^{-1}$ , testing RE was below 3.6% and  $R^2$  was at least equal to 96%. According to the literature, those values are considered very good to excellent. For example, Rahimikhoob (2010) recommended an ANN for the coastal area of the Caspian Sea in Northern Iran, which used only air temperature as an input, with an  $\text{RMSE} = 0.41 \text{ mm d}^{-1}$  and  $R^2 = 95\%$  [84], whereas in this study MLP14 with  $T_{\text{mean}}$  as an input has better accuracy ( $\text{RMSE} = 0.360 \text{ mm d}^{-1}$  and  $R^2 = 96.9\%$ ). In the same vein, Zanetti et al. (2008) used MLP ANN with only temperature and radiation inputs to predict  $E_{\text{To}}$  for Campos dos Goytacazes, Brazil [66], while Ravindran et al. (2021) deduced that  $R_s$  was the most influential parameter to  $E_{\text{To}}$  and used it as a sole input in ANNs for California ( $R^2$  up to 95.4%) [14]. This proves that ANNs with simple architecture can be good predictive models of  $E_{\text{To}}$  over the Peloponnese for the examined period. In addition, based on the best ANN model (MLP1), we found that  $T_{\text{mean}}$  and  $u_2$  were the two most influential factors on  $E_{\text{To}}$ , out of the seven examined. This is in line with the findings of a previous study of the same period for the Peloponnese, where  $E_{\text{To}}$  had been computed by FAO PM [63].  $T_{\text{mean}}$ , as a proxy of the energy state of the system, is one of the most influential factors on  $E_{\text{To}}$ . This depicts the altitude and land cover difference over short distances across the Peloponnese. Probably, due to the fact that the Peloponnese has a very low variance in latitude, the radiation factors were not that influential for the determination of the  $E_{\text{To}}$ . Regarding the second most influential factor ( $u_2$ ), in contrast with December (winter), increased values of  $u_2$  are not frequent in Greece during August (summer). Therefore, where increased  $u_2$  values occurred in August, they affected the determination of the local  $E_{\text{To}}$  values. In conclusion, ANNs resulted in predictions very close to FAO PM, which is the most established reference method, for the examined period for the Peloponnese. Therefore, ANNs present the potential of general usage in modeling  $E_{\text{To}}$  across Greece, after further investigation.

This study proves that ANNs can be useful alternatives for predicting  $E_{\text{To}}$ , requiring limited climate data as input. The former is of considerable usefulness in cases where climate data are in shortage or the cost of the meteorological stations is not affordable, such as in developing countries. Despite the cost, ANNs provide a time saving and a computational effort-decreasing alternative to the complex algorithms currently used, which is applicable for interdisciplinary research purposes.

## 5. Conclusions

Among the tested ANNs, MLPs performed generally better than RBFs for multiple inputs, whereas RBFs performed slightly better when one sole input ( $R_n$  or  $T_{\text{mean}}$ ) was set. The results revealed better performance of the MLP1 7-2 model, with all the available

variables as inputs and only one hidden layer, bearing an RMSE = 0.290 mm d<sup>-1</sup>, R<sup>2</sup> = 98% and RE values of testing and validation phases equal to 2.7% and 2.2%, respectively. The former proves that even simple ANN architectures can constitute very satisfactory predicting models. Models with only two parameters as inputs exhibited RMSE values up to 0.352 mm d<sup>-1</sup> and R<sup>2</sup> values at least equal to 97% (MLP6, MLP13). When one sole input was used (Tmean or Rn) in RBF models, RMSE was below 0.385 mm d<sup>-1</sup> and R<sup>2</sup> was at least equal to 96%. The results in both cases are very satisfactory. The MLP1, which outperformed the rest of the ANNs, determined the order of importance of parameters that affect ETo. The first two most influential parameters were Tmean and u<sub>2</sub>. Tmean is commonly a parameter to which ETo variances are attributed, as it depicts the overall energy state of the system. For the Peloponnese, where the variance of the latitude (and consequently of solar radiation) values is minor, Tmean variances occur mostly due to distinguished differences in relief, LU/LC types and proximity to the coast over short distances. Wind speed (u<sub>2</sub>) plays a substantial role, especially in August, when any increased u<sub>2</sub> values directly affect the ETo values, since those are not frequent in summertime. Future research could test the MLP1 performance for a larger period and across different areas of Greece that differentiate in micro-climatic conditions and regimes. Moreover, direct measurements such as pan evaporation measurements employing ANNs could be investigated on a local scale. Another interesting idea, based on the satisfactory results of this study regarding a sole input variable, would be to explore the potential of multilinear regression analysis, which is a simpler method and comprehensible by a wider interdisciplinary audience.

**Author Contributions:** Conceptualization, S.D. and K.G.N.; methodology, S.D. and K.G.N.; software, S.D.; validation S.D.; formal analysis, S.D.; investigation, S.D., data curation, S.D., writing—original draft preparation, S.D., writing and editing, S.D. and K.G.N.; supervision, K.G.N. All authors have read and agreed to the published version of the manuscript.

**Funding:** This research received no external funding.

**Institutional Review Board Statement:** Not applicable.

**Informed Consent Statement:** Not applicable.

**Data Availability Statement:** Data are private, available only for the review process of the present article.

**Acknowledgments:** The authors acknowledge the National Observatory of Athens (<https://meteosearch.meteo.gr> (accessed on 15 April 2022)) for ground-based data availability of sixty-two meteorological stations.

**Conflicts of Interest:** The authors declare no conflict of interest.

## Appendix A

**Table A1.** Meteorological stations (62) used (source: <https://meteosearch.meteo.gr> (accessed on 15 April 2022)).

ID	Station	X	Y	Elevation (m)	Municipality	ID	Station	X	Y	Elevation (m)	Municipality
Meteorological Stations for the 3 Empirical Methods (ETo)						Meteorological Stations for the 3 Empirical Methods (ETo)					
1	Kalavrita	334349.9	4210128	781	Achaia	32	Oleni	282783.4	4177872	61	Ilia
2	Kato Vlassia	317683.4	4208558	773	Achaia	33	Pineia	285425.3	4191240	184	Ilia
3	Lappa	273550	4218928	15	Achaia	34	Pirgos	273886.9	4171891	22	Ilia
4	Olenia	288845.1	4221654	34	Achaia	35	Vartholomio	253773.8	4193127	15	Ilia
5	Panachaiko	313491.4	4235800	1588	Achaia	36	Zacharo	290302.6	4150806	5	Ilia

Table A1. Cont.

ID	Station	X	Y	Elevation (m)	Municipality	ID	Station	X	Y	Elevation (m)	Municipality
Meteorological Stations for the 3 Empirical Methods (ETo)						Meteorological Stations for the 3 Empirical Methods (ETo)					
6	Panagopoula	318709.5	4243842	15	Achaia	37	Amoni Sofikou	424227.5	4186898	55	Korinthia
7	Panepistimio	305972.3	4239289	66	Achaia	38	Derveni	362057.1	4221737	5	Korinthia
8	Patra	301697.8	4236694	6	Achaia	39	Isthmos	408645.4	4200499	6	Korinthia
9	Rio	305898.1	4242177	2	Achaia	40	Kiato	389163.5	4207722	15	Korinthia
10	Romanos	313476.1	4235744	228	Achaia	41	Krioneri	378491.9	4203310	887	Korinthia
11	Sageika	280638.4	4219575	26	Achaia	42	Loutraki	410248.7	4202636	30	Korinthia
12	Argos	386329.1	4165059	38	Argolida	43	Nemea	381197.9	4188976	290	Korinthia
13	Didima	426936.9	4146702	175	Argolida	44	Perigiali	397303.1	4199344	38	Korinthia
14	Kranidi	424615.7	4137411	110	Argolida	45	Trikala Korinthias	365493.7	4206835	1077	Korinthia
15	Lagadia	326139.9	4172057	970	Arkadia	46	Agioi Theodoroi	423533.6	4198395	37	Korinthia
16	Levidi	349386.5	4171330	853	Arkadia	47	Apidia	392819.7	4082655	230	Lakonia
17	Lykochia	337772.6	4151113	870	Arkadia	48	Asteri	386527.1	4076757	8	Lakonia
18	Magouliana	334497.7	4171275	1256	Arkadia	49	Geraki	384706.6	4094508	330	Lakonia
19	Megalopoli	335363	4140782	432	Arkadia	50	Krokees	371576.2	4082640	241	Lakonia
20	Stemnitsa	330377.8	4157967	1094	Arkadia	51	Molaoi	397984.6	4072957	128	Lakonia
21	Tripoli	359989.3	4152250	650	Arkadia	52	Monemvasia	413811.4	4059051	17	Lakonia
22	Vytina	339989.8	4170409	1013	Arkadia	53	Sparti	360929.9	4101670	204	Lakonia
23	Spetses	424919.5	4124662	3	Attiki	54	Alagonia	343840.9	4107863	765	Messinia
24	Taktikoupoli Troizinias	443373.2	4152374	15	Attiki	55	Arfara	326299.4	4113666	96	Messinia
25	Ydra	452645.8	4133727	2	Attiki	56	Filiatra	285439.9	4115175	65	Messinia
26	Amaliada	264604.9	4186923	26	Iliia	57	Kalamata	331127	4098974	5	Messinia
27	Andritsaina	314220.3	4152125	731	Iliia	58	Kalamata Dytika	329347.3	4100001	10	Messinia
28	Archaia Olympia	287981.3	4163856	45	Iliia	59	Kardamili	347857.7	4074651	13	Messinia
29	Foloi	297082.7	4174732	600	Iliia	60	Kopanaki	306288.6	4128741	184	Messinia
30	Katakolo	263537.2	4169327	2	Iliia	61	Kyparissia	291691	4123584	36	Messinia
31	Lampeia	306840.3	4192041	840	Iliia	62	Pylos	294556.8	4087590	5	Messinia

## References

1. Malamos, N.; Tegos, A. Advances in Evaporation and Evaporative Demand. *Hydrology* **2022**, *9*, 78. [[CrossRef](#)]
2. Shamshirband, S.; Hashemi, S.; Salimi, H.; Samadianfard, S.; Asadi, E.; Shadkani, S.; Kargar, K.; Mosavi, A.; Nabipour, N.; Chau, K.W. Predicting Standardized Streamflow index for hydrological drought using machine learning models. *Eng. Appl. Comput. Fluid Mech.* **2020**, *14*, 339–350. [[CrossRef](#)]
3. Xu, S.; Yu, Z.; Yang, C.; Ji, X.; Zhang, K. Trends in evapotranspiration and their responses to climate change and vegetation greening over the upper reaches of the Yellow River Basin. *Agric. For. Meteorol.* **2018**, *263*, 118–129. [[CrossRef](#)]
4. Dimitriadou, S.; Nikolakopoulos, K.G. Evapotranspiration Trends and Interactions in Light of the Anthropogenic Footprint and the Climate Crisis: A Review. *Hydrology* **2021**, *8*, 163. [[CrossRef](#)]
5. Pereira, L.S.; Perrier, A.; Allen, R.G.; Alves, I. Evapotranspiration: Concepts and Future Trends. *J. Irrig. Drain. Eng.* **1999**, *125*, 45–51. [[CrossRef](#)]
6. Malamos, N.; Tsirogiannis, I.L.; Tegos, A.; Efstratiadis, A.; Koutsoyiannis, D. Spatial interpolation of potential evapotranspiration for precision irrigation purposes. *Eur. Water* **2017**, *59*, 303–309.
7. Saggi, M.K.; Jain, S. Reference evapotranspiration estimation and modeling of the Punjab Northern India using deep learning. *Comput. Electron. Agric.* **2019**, *156*, 387–398. [[CrossRef](#)]
8. Zhang, Y.; Wei, Z.; Zhang, L.; Du, J. Applicability evaluation of different algorithms for daily reference evapotranspiration model in KBE system. *Int. J. Comput. Sci. Eng.* **2019**, *18*, 361–374. [[CrossRef](#)]
9. Li, M.; Chu, R.; Islam, A.R.M.T.; Shen, S. Reference Evapotranspiration Variation Analysis and Its Approaches Evaluation of 13 Empirical Models in Sub-Humid and Humid Regions: A Case Study of the Huai River Basin, Eastern China. *Water* **2018**, *10*, 493. [[CrossRef](#)]

10. Tabari, H.; Grismer, M.E.; Trajkovic, S. Comparative analysis of 31 reference evapotranspiration methods under humid conditions. *Irrig. Sci.* **2013**, *31*, 107–117. [[CrossRef](#)]
11. Roy, D.K.; Sarkar, T.K.; Alam Kamar, S.S.; Goswami, T.; Muktadir, A.; Al-Ghobari, H.M.; Alataway, A.; Dewidar, A.Z.; El-Shafei, A.A.; Mattar, M.A. Daily Prediction and Multi-Step Forward Forecasting of Reference Evapotranspiration Using LSTM and Bi-LSTM Models. *Agronomy* **2022**, *12*, 594. [[CrossRef](#)]
12. Ferreira, L.B.; da Cunha, F.F. Multi-step ahead forecasting of daily reference evapotranspiration using deep learning. *Comput. Electron. Agric.* **2020**, *178*, 105728. [[CrossRef](#)]
13. Ravindran, S.M.; Bhaskaran, S.K.M.; Ambat, S.K.N. A Deep Neural Network Architecture to Model Reference Evapotranspiration Using a Single Input Meteorological Parameter. *Environ. Process.* **2021**, *8*, 1567–1599. [[CrossRef](#)]
14. Granata, F.; Di Nunno, F. Forecasting evapotranspiration in different climates using ensembles of recurrent neural networks. *Agric. Water Manag.* **2021**, *255*, 107040. [[CrossRef](#)]
15. Mosavi, A.; Edalatifar, M. A Hybrid Neuro-Fuzzy Algorithm for Prediction of Reference Evapotranspiration. In *Recent Advances in Technology Research and Education*; Laukaitis, G., Ed.; INTER-ACADEMIA 2018; Lecture Notes in Networks and Systems; Springer: Cham, Switzerland, 2019; Volume 53. [[CrossRef](#)]
16. Andreu, A.; Kustas, W.P.; Polo, M.J.; Carrara, A.; González-Dugo, M.P. Modeling Surface Energy Fluxes over a Dehesa (Oak Savanna) Ecosystem Using a Thermal Based Two Source Energy Balance Model (TSEB) II—Integration of Remote Sensing Medium and Low Spatial Resolution Satellite Images. *Remote Sens.* **2018**, *10*, 558. [[CrossRef](#)]
17. Silva, A.M.; da Silva, R.M.; Santos, C.A.G. Automated surface energy balance algorithm for land (ASEBAL) based on automating endmember pixel selection for evapotranspiration calculation in MODIS orbital images. *Int. J. Appl. Earth Obs. Geoinf.* **2019**, *79*, 1–11. [[CrossRef](#)]
18. Zakeri, M.S.; Mousavi, S.F.; Farzin, S.; Sanikhani, H. Modeling of Reference Crop Evapotranspiration in Wet and Dry Climates Using Data-Mining Methods and Empirical Equations. *J. Soft Comput. Civ. Eng.* **2022**, *6*, 1–28. [[CrossRef](#)]
19. Achite, M.; Jehanzaib, M.; Sattari, M.T.; Toubal, A.K.; Elshaboury, N.; Wałęga, A.; Krakauer, N.; Yoo, J.-Y.; Kim, T.-W. Modern Techniques to Modeling Reference Evapotranspiration in a Semiarid Area Based on ANN and GEP Models. *Water* **2022**, *14*, 1210. [[CrossRef](#)]
20. Elbeltagi, A.; Kumar, N.; Chandel, A.; Arshad, A.; Pande, C.B.; Islam, A.R.M.T. Modelling the reference crop evapotranspiration in the Beas-Sutlej basin (India): An artificial neural network approach based on different combinations of meteorological data. *Environ. Monit. Assess.* **2022**, *194*, 141. [[CrossRef](#)]
21. Elbeltagi, A.; Kushwaha, N.L.; Rajput, J.; Vishwakarma, D.K.; Kulimushi, L.C.; Kumar, M.; Zhang, J.; Pande, C.B.; Choudhari, P.; Meshram, S.G.; et al. Modelling daily reference evapotranspiration based on stacking hybridization of ANN with meta-heuristic algorithms under diverse agro-climatic conditions. *Stoch. Hydrol. Hydraul.* **2022**, 1–24. [[CrossRef](#)]
22. Long, X.; Wang, J.; Gong, S.; Li, G.; Ju, H. Reference evapotranspiration estimation using long short-term memory network and wavelet-coupled long short-term memory network. *Irrig. Drain.* **2022**. [[CrossRef](#)]
23. Chia, M.Y.; Huang, Y.F.; Koo, C.H. ANN-Based Reference Evapotranspiration Estimation: Effects of Data Normalization and Parameters Selection. In *Proceedings of International Conference on Emerging Technologies and Intelligent Systems*; Al-Emran, M., Al-Sharafi, M.A., Al-Kabi, M.N., Shaalan, K., Eds.; ICETIS 2021; Lecture Notes in Networks and Systems; Springer: Cham, Switzerland, 2022; pp. 3–12. [[CrossRef](#)]
24. Ferreira, L.B.; da Cunha, F.F.; Filho, E.I.F. Exploring machine learning and multi-task learning to estimate meteorological data and reference evapotranspiration across Brazil. *Agric. Water Manag.* **2022**, *259*, 107281. [[CrossRef](#)]
25. Manikumari, N.; Vinodhini, G.; Murugappan, A. Modelling of Reference Evapotranspiration using Climatic Parameters for Irrigation Scheduling using Machine learning. *ISH J. Hydraul. Eng.* **2022**, *28*, 272–281. [[CrossRef](#)]
26. Krishnashetty, P.H.; Balasangameshwara, J.; Sreeman, S.; Desai, S.; Kantharaju, A.B. Cognitive computing models for estimation of reference evapotranspiration: A review. *Cogn. Syst. Res.* **2021**, *70*, 109–116. [[CrossRef](#)]
27. Algretawee, H.; Alshama, G. Modeling of Evapotranspiration (ET<sub>o</sub>) in a Medium Urban Park within a Megacity by Using Artificial Neural Network (ANN) Model. *Period. Polytech. Civ. Eng.* **2021**, *65*, 1260–1268. [[CrossRef](#)]
28. Gao, L.; Gong, D.; Cui, N.; Lv, M.; Feng, Y. Evaluation of bio-inspired optimization algorithms hybrid with artificial neural network for reference crop evapotranspiration estimation. *Comput. Electron. Agric.* **2021**, *190*, 106466. [[CrossRef](#)]
29. Yurtseven, I.; Serengil, Y. Comparison of different empirical methods and data-driven models for estimating reference evapotranspiration in semi-arid Central Anatolian Region of Turkey. *Arab. J. Geosci.* **2021**, *14*, 2033. [[CrossRef](#)]
30. He, Y.; Lin, E.S.; Tan, C.L.; Tan, P.Y.; Wong, N.H. Quantitative evaluation of plant evapotranspiration effect for green roof in tropical area: A case study in Singapore. *Energy Build.* **2021**, *241*, 110973. [[CrossRef](#)]
31. Gocić, M.; Amiri, M.A. Reference Evapotranspiration Prediction Using Neural Networks and Optimum Time Lags. *Water Resour. Manag.* **2021**, *35*, 1913–1926. [[CrossRef](#)]
32. del Cerro, R.T.G.; Subathra, M.; Kumar, N.M.; Verrastro, S.; George, S.T. Modelling the daily reference evapotranspiration in semi-arid region of South India: A case study comparing ANFIS and empirical models. *Inf. Process. Agric.* **2020**, *8*, 173–184. [[CrossRef](#)]
33. Khedkar, D.D.; Singh, P.K. Comparison of neural network models for estimation of reference crop evapotranspiration. *Agric. Res. J.* **2021**, *58*, 60–67. [[CrossRef](#)]

34. Abdullahi, J.; Rotimi, A.; Malami, S.I.; Jibrin, H.B.; Tahsin, A.; Abba, S. Feasibility of artificial intelligence and CROPWAT models in the estimation of uncertain combined variable using nonlinear sensitivity analysis. In Proceedings of the 2021 1st International Conference on Multidisciplinary Engineering and Applied Science (ICMEAS), Abuja, Nigeria, 15–16 July 2021; pp. 1–7. [\[CrossRef\]](#)
35. Reddy, K.C. Machine Intelligence-Based Reference Evapotranspiration Modelling: An application of Neural Networks. In Proceedings of the 2021 International Conference on Artificial Intelligence and Machine Vision (AIMV), Gandhinagar, India, 24–26 September 2021; pp. 1–5. [\[CrossRef\]](#)
36. Nawandar, N.K.; Cheggoju, N.; Satpute, V. ANN-Based Model to Predict Reference Evapotranspiration for Irrigation Estimation. In *Advances in Intelligent Systems and Computing: Proceedings of International Conference on Recent Trends in Machine Learning, IoT, Smart Cities and Applications*; Gunjan, V.K., Zurada, J.M., Eds.; Springer: Singapore, 2021; Volume 1245, pp. 671–679. [\[CrossRef\]](#)
37. Yamaç, S.S. Reference evapotranspiration estimation with k-Nearest Neighbour and Artificial neural network models using different climate input variables in the semi-arid environment. *J. Agric. Sci.* **2021**, *27*, 129–137. [\[CrossRef\]](#)
38. Ferreira, L.B.; da Cunha, F.F.; da Silva, G.H.; Campos, F.B.; Dias, S.H.B.; Santos, J.E.O. Generalizability of machine learning models and empirical equations for the estimation of reference evapotranspiration from temperature in a semiarid region. *Anais da Academia Brasileira de Ciências* **2021**, *93*, e20200304. [\[CrossRef\]](#)
39. Yu, H.; Wen, X.; Li, B.; Yang, Z.; Wu, M.; Ma, Y. Uncertainty analysis of artificial intelligence modeling daily reference evapotranspiration in the northwest end of China. *Comput. Electron. Agric.* **2020**, *176*, 105653. [\[CrossRef\]](#)
40. Maroufpoor, S.; Bozorg-Haddad, O.; Maroufpoor, E. Reference evapotranspiration estimating based on optimal input combination and hybrid artificial intelligent model: Hybridization of artificial neural network with grey wolf optimizer algorithm. *J. Hydrol.* **2020**, *588*, 125060. [\[CrossRef\]](#)
41. Alizamir, M.; Kisi, O.; Adnan, R.M.; Kuriqi, A. Modelling reference evapotranspiration by combining neuro-fuzzy and evolutionary strategies. *Acta Geophys.* **2020**, *68*, 1113–1126. [\[CrossRef\]](#)
42. Tikhamarine, Y.; Malik, A.; Souag-Gamane, D.; Kisi, O. Artificial intelligence models versus empirical equations for modeling monthly reference evapotranspiration. *Environ. Sci. Pollut. Res.* **2020**, *27*, 30001–30019. [\[CrossRef\]](#)
43. Seifi, A.; Riahi, H. Estimating daily reference evapotranspiration using hybrid gamma test-least square support vector machine, gamma test-ANN, and gamma test-ANFIS models in an arid area of Iran. *J. Water Clim. Chang.* **2020**, *11*, 217–240. [\[CrossRef\]](#)
44. Nourani, V.; Elkiran, G.; Abdullahi, J. Multi-step ahead modeling of reference evapotranspiration using a multi-model approach. *J. Hydrol.* **2019**, *581*, 124434. [\[CrossRef\]](#)
45. Zhu, B.; Feng, Y.; Gong, D.; Jiang, S.; Zhao, L.; Cui, N. Hybrid particle swarm optimization with extreme learning machine for daily reference evapotranspiration prediction from limited climatic data. *Comput. Electron. Agric.* **2020**, *173*, 105430. [\[CrossRef\]](#)
46. Reis, M.M.; Silva, A.; Junior, J.Z.; Santos, L.T.; Azevedo, A.M.; Lopes, M.G. Empirical and learning machine approaches to estimating reference evapotranspiration based on temperature data. *Comput. Electron. Agric.* **2019**, *165*, 104937. [\[CrossRef\]](#)
47. Ferreira, L.B.; da Cunha, F.F.; de Oliveira, R.A.; Filho, E.I.F. Estimation of reference evapotranspiration in Brazil with limited meteorological data using ANN and SVM—A new approach. *J. Hydrol.* **2019**, *572*, 556–570. [\[CrossRef\]](#)
48. Sidiropoulos, P.; Dalezios, N.R.; Loukas, A.; Mylopoulos, N.; Spiliotopoulos, M.; Faraslis, I.N.; Alpanakis, N.; Sakellariou, S. Quantitative Classification of Desertification Severity for Degraded Aquifer Based on Remotely Sensed Drought Assessment. *Hydrology* **2021**, *8*, 47. [\[CrossRef\]](#)
49. Raoufi, R.; Beighley, E. Estimating Daily Global Evapotranspiration Using Penman–Monteith Equation and Remotely Sensed Land Surface Temperature. *Remote Sens.* **2017**, *9*, 1138. [\[CrossRef\]](#)
50. Allen, R.G.; Tasumi, M.; Trezza, R. Satellite-Based Energy Balance for Mapping Evapotranspiration with Internalized Calibration (METRIC)—Model. *J. Irrig. Drain. Eng.* **2007**, *133*, 380–394. [\[CrossRef\]](#)
51. Dimitriadou, S.; Nikolakopoulos, K.G. Remote sensing methods to estimate evapotranspiration incorporating MODIS de-rived data and applications over Greece: A review. In Proceedings of the SPIE 11524, Eighth International Conference on Remote Sensing and Geoinformation of the Environment (RSCy2020), Paphos, Cyprus, 26 August 2020. [\[CrossRef\]](#)
52. Liu, Y.; Zhang, S.; Zhang, J.; Tang, L.; Bai, Y. Assessment and Comparison of Six Machine Learning Models in Estimating Evapotranspiration over Croplands Using Remote Sensing and Meteorological Factors. *Remote Sens.* **2021**, *13*, 3838. [\[CrossRef\]](#)
53. Proias, G.; Gravalos, I.; Papageorgiou, E.; Poczęta, K.; Sakellariou-Makrantonaki, M. Forecasting Reference Evapotranspiration Using Time Lagged Recurrent Neural Network. *WSEAS Trans. Environ. Dev.* **2020**, *16*, 699–707. [\[CrossRef\]](#)
54. Kitsara, G.; Papaioannou, G.; Retalis, A.; Paronis, D.; Kerkides, P. Estimation of air temperature and reference evapotranspiration using MODIS land surface temperature over Greece. *Int. J. Remote Sens.* **2018**, *39*, 924–948. [\[CrossRef\]](#)
55. Falalakis, G.; Gemtzi, A. A simple method for water balance estimation based on the empirical method and remotely sensed evapotranspiration estimates. *J. Hydroinform.* **2020**, *22*, 440–451. [\[CrossRef\]](#)
56. Tsouni, A.; Kontoes, C.; Koutsoyiannis, D.; Elias, P.; Mamassis, N. Estimation of Actual Evapotranspiration by Remote Sensing: Application in Thessaly Plain, Greece. *Sensors* **2008**, *8*, 3586–3600. [\[CrossRef\]](#)
57. Vasiliades, L.; Spiliotopoulos, M.; Tzabiras, J.; Loukas, A.; Mylopoulos, N. Estimation of crop water requirements using remote sensing for operational water resources management. In Proceedings of the Third International Conference on Remote Sensing and Geoinformation of the Environment (RSCy2015), Paphos, Cyprus, 19 June 2015. [\[CrossRef\]](#)
58. Dimitriadou, S.; Nikolakopoulos, K.G. Development of GIS models via optical programming and python scripts to implement four empirical methods of reference and actual evapotranspiration (ET<sub>o</sub>, ET<sub>a</sub>) incorporating MODIS LST inputs. In Proceedings of the SPIE 11856, Remote Sensing for Agriculture, Ecosystems, and Hydrology XXIII, Madrid, Spain, 12 September 2021. [\[CrossRef\]](#)

59. Allen, R.; Pereira, L.; Raes, D.; Smith, M. *Crop Evapotranspiration-Guidelines for Computing Crop Water Requirements-FAO Irrigation and Drainage Paper 56*; FAO: Rome, Italy, 1998; Volume 300, p. D05109.
60. Pereira, L.S.; Allen, R.G.; Smith, M.; Raes, D. Crop evapotranspiration estimation with FAO56: Past and future. *Agric. Water Manag.* **2015**, *147*, 4–20. [[CrossRef](#)]
61. Valiantzas, J.D. Simplified Reference Evapotranspiration Formula Using an Empirical Impact Factor for Penman's Aerodynamic Term. *J. Hydrol. Eng.* **2013**, *18*, 108–114. [[CrossRef](#)]
62. Djaman, K.; Rudnick, D.; Mel, V.C.; Mutiibwa, D.; Diop, L.; Sall, M.; Kabenge, I.; Bodian, A.; Tabari, H.; Irmak, S. Evaluation of Valiantzas' Simplified Forms of the FAO-56 Penman-Monteith Reference Evapotranspiration Model in a Humid Climate. *J. Irrig. Drain. Eng.* **2017**, *143*, 06017005. [[CrossRef](#)]
63. Dimitriadou, S.; Nikolakopoulos, K.G. Reference Evapotranspiration (ET<sub>0</sub>) Methods Implemented as ArcMap Models with Remote-Sensed and Ground-Based Inputs, Examined along with MODIS ET, for Peloponnese, Greece. *ISPRS Int. J. Geo-Inf.* **2021**, *10*, 390. [[CrossRef](#)]
64. Tegos, A.; Efstratiadis, A.; Malamos, N.; Mamassis, N.; Koutsoyiannis, D. Evaluation of a Parametric Approach for Estimating Potential Evapotranspiration Across Different Climates. *Agric. Agric. Sci. Procedia* **2015**, *4*, 2–9. [[CrossRef](#)]
65. Zanetti, S.S.; Sousa, E.F.; Oliveira, V.P.S.; Almeida, F.T.; Bernardo, S. Estimating Evapotranspiration Using Artificial Neural Network and Minimum Climatological Data. *J. Irrig. Drain. Eng.* **2007**, *133*, 83–89. [[CrossRef](#)]
66. ASCE Task Committee on Application of Artificial Neural Networks in Hydrology. Artificial neural networks in hydrology. I: Preliminary concepts. *J. Hydrol. Eng.* **2000**, *5*, 115–123. [[CrossRef](#)]
67. Shakiba, F.M.; Zhou, M. Novel Analog Implementation of a Hyperbolic Tangent Neuron in Artificial Neural Networks. *IEEE Trans. Ind. Electron.* **2020**, *68*, 10856–10867. [[CrossRef](#)]
68. Huss, M.; Farinotti, D.; Bauder, A.; Funk, M. Modelling runoff from highly glacierized alpine drainage basins in a changing climate. *Hydrol. Process.* **2009**, *2274*, 2267–2274. [[CrossRef](#)]
69. Trajkovic, S.; Todorovic, B.; Stankovic, M. Forecasting of Reference Evapotranspiration by Artificial Neural Networks. *J. Irrig. Drain. Eng.* **2003**, *129*, 454–457. [[CrossRef](#)]
70. Kumar, N.; Maharshi, S.; Poddar, A.; Shankar, V. Evaluation of Artificial Neural Networks for Estimating Reference Evapotranspiration in Western Himalayan Region. In Proceedings of the 2020 International Conference on Computational Performance Evaluation (ComPE), Shillong, India, 2–4 July 2020; pp. 163–167. [[CrossRef](#)]
71. Tabari, H.; Talaei, P.H. Multilayer perceptron for reference evapotranspiration estimation in a semiarid region. *Neural Comput. Appl.* **2012**, *23*, 341–348. [[CrossRef](#)]
72. Shamshirband, S.; Amirmojahedi, M.; Gocić, M.; Akib, S.; Petković, D.; Piri, J.; Trajkovic, S. Estimation of Reference Evapotranspiration Using Neural Networks and Cuckoo Search Algorithm. *J. Irrig. Drain. Eng.* **2016**, *142*, 04015044. [[CrossRef](#)]
73. Sattari, M.T.; Apaydin, H.; Band, S.S.; Mosavi, A.; Prasad, R. Comparative analysis of kernel-based versus ANN and deep learning methods in monthly reference evapotranspiration estimation. *Hydrol. Earth Syst. Sci.* **2021**, *25*, 603–618. [[CrossRef](#)]
74. Gavili, S.; Sanikhani, H.; Kisi, O.; Mahmoudi, M.H. Evaluation of several soft computing methods in monthly evapotranspiration modelling. *Meteorol. Appl.* **2017**, *25*, 128–138. [[CrossRef](#)]
75. Diamantopoulou, M.J.; Georgiou, P.E.; Papamichail, D.M. Performance evaluation of artificial neural networks in estimating reference evapotranspiration with minimal meteorological data. *Glob. NEST J.* **2011**, *13*, 18–27.
76. Antonopoulos, V.Z.; Gianniu, S.K.; Antonopoulos, A.V. Artificial neural networks and empirical equations to estimate daily evaporation: Application to Lake Vegorititis, Greece. *Hydrol. Sci. J.* **2016**, *61*, 2590–2599. [[CrossRef](#)]
77. Antonopoulos, V.Z.; Antonopoulos, A.V. Daily reference evapotranspiration estimates by artificial neural networks technique and empirical equations using limited input climate variables. *Comput. Electron. Agric.* **2017**, *132*, 86–96. [[CrossRef](#)]
78. Dimitriadou, S.; Katsanou, K.; Charalabopoulos, S.; Lambrakis, N. Interpretation of the Factors Defining Groundwater Quality of the Site Subjected to the Wildfire of 2007 in Ilia Prefecture, South-Western Greece. *Geosciences* **2018**, *8*, 108. [[CrossRef](#)]
79. Copernicus Land Monitoring Service. CLC 2018. ©European Union, Copernicus Land Monitoring Service 2018, European Environment Agency (EEA). Available online: <https://land.copernicus.eu/pan-european/corine-land-cover/clc2018> (accessed on 11 April 2022).
80. Kotteck, M.; Grieser, J.; Beck, C.; Rudolf, B.; Rubel, F. World map of the Köppen-Geiger climate classification updated. *Meteorol. Z.* **2006**, *15*, 259–263. [[CrossRef](#)]
81. Elbeltagi, A.; Nagy, A.; Mohammed, S.; Pande, C.B.; Kumar, M.; Bhat, S.A.; Zsembeli, J.; Huzsvai, L.; Tamás, J.; Kovács, E.; et al. Combination of Limited Meteorological Data for Predicting Reference Crop Evapotranspiration Using Artificial Neural Network Method. *Agronomy* **2022**, *12*, 516. [[CrossRef](#)]
82. Abrishami, N.; Sepaskhah, A.R.; Shahrokhnia, M.H. Estimating wheat and maize daily evapotranspiration using artificial neural network. *Arch. Meteorol. Geophys. Bioclimatol. Ser. B* **2019**, *135*, 945–958. [[CrossRef](#)]
83. Kisi, O.; Sanikhani, H.; Zounemat-Kermani, M.; Niazi, F. Long-term monthly evapotranspiration modeling by several data-driven methods without climatic data. *Comput. Electron. Agric.* **2015**, *115*, 66–77. [[CrossRef](#)]
84. Rahimikhoo, A. Estimation of evapotranspiration based on only air temperature data using artificial neural networks for a subtropical climate in Iran. *Arch. Meteorol. Geophys. Bioclimatol. Ser. B* **2010**, *101*, 83–91. [[CrossRef](#)]

85. Gomar, S.; Mirhassani, M.; Ahmadi, M. Precise digital implementations of hyperbolic tanh and sigmoid function. In Proceedings of the 2016 50th Asilomar Conference on Signals, Systems and Computers, Pacific Grove, CA, USA, 6–9 November 2016; pp. 1586–1589. [\[CrossRef\]](#)
86. Genaidy, M.A. Estimating of evapotranspiration using artificial neural network. *Misr. J. Agric. Eng.* **2020**, *37*, 81–94. Available online: [https://mjae.journals.ekb.eg/article\\_94971\\_382909fe6190f50b2edcab1dc6d3c8b9.pdf](https://mjae.journals.ekb.eg/article_94971_382909fe6190f50b2edcab1dc6d3c8b9.pdf) (accessed on 15 May 2022). [\[CrossRef\]](#)
87. Cococcioni, M.; Rossi, F.; Ruffaldi, E.; Saponara, S. A Fast Approximation of the Hyperbolic Tangent When Using Posit Numbers and Its Application to Deep Neural Networks. In *Applications in Electronics Pervading Industry, Environment and Society*; Saponara, S., De Gloria, A., Eds.; ApplePies. Lecture Notes in Electrical Engineering; Springer: Cham, Switzerland, 2019; Volume 627, pp. 213–221. [\[CrossRef\]](#)